# Complete description of ionization energy and electron affinity in organic solids: Determining contributions from electronic polarization, energy band dispersion, and molecular orientation

Hiroyuki Yoshida,[1,*] Kazuto Yamada,[1] Jun'ya Tsutsumi,[2] and Naoki Sato[1]

[1]*Institute for Chemical Research, Kyoto University, Uji, Kyoto 611-001, Japan*

[2]*Flexible Electronics Research Center, National Institute of Advanced Industrial Science and Technology, 1-1-1 Higashi, Tsukuba 305-8562, Japan*

(Received 25 February 2015; revised manuscript received 16 July 2015; published 31 August 2015)

Ionization energy and electron affinity in organic solids are understood in terms of a single molecule perturbed by solid-state effects such as polarization energy, band dispersion, and molecular orientation as primary factors. However, no work has been done to determine the individual contributions experimentally. In this work, the electron affinities of thin films of pentacene and perfluoropentacene with different molecular orientations are determined to a precision of 0.1 eV using low-energy inverse photoemission spectroscopy. Based on the precisely determined electron affinities in the solid state together with the corresponding data of the ionization energies and other energy parameters, we quantitatively evaluate the contribution of these effects. It turns out that the bandwidth as well as the polarization energy contributes to the ionization energy and electron affinity in the solid state while the effect of the surface dipole is at most a few eV and does not vary with the molecular orientation. As a result, we conclude that the molecular orientation dependence of the ionization energy and electron affinity of organic solids originates from the orientation-dependent polarization energy in the film.

DOI: 10.1103/PhysRevB.92.075145 PACS number(s): 73.61.Ph, 71.20.Rv, 79.60.Dp

## I. INTRODUCTION

The behavior of charge carriers in solid-state organic materials anchored by $\pi$-conjugated molecules is of fundamental importance to their application to electronic devices. The electronic levels of charge carriers in the occupied and unoccupied states are characterized by ionization energy, $I$, and electron affinity, $A$, respectively, in the solid state. $I$ and $A$ are governed by various effects that the charge carriers experience in the organic media, such as the electrostatic relaxation, the intermolecular orbital interaction, and the local electronic field. Analyzing and distinguishing these contributions gives a clue to elucidate the charge carrier behaviors in organic solid.

Organic solids consist of molecules bound by weak intermolecular interactions such as van der Waals and electrostatic forces. Their electronic energy levels are therefore understood in terms of those of an isolated molecule perturbed by the weak intermolecular interactions [1,2]. This was demonstrated by a similarity between photoelectron spectra in the gas (isolated molecule) and solid phases [3,4]. The observed small differences were interpreted in terms of the polarization effect which originates from the screening of the positive charge (cation) generated in the photoemission process caused by the electronic polarization of the surrounding molecules. $I$ and $A$ in the gas and solid phases were connected with the polarization energies $P_+$ and $P_-$ for positive and negative charges, respectively, by the following formula [1,5]:

$$I_s = I_g - P_+, \quad A_s = A_g + P_-, \tag{1}$$

where the subscripts g and s refer to the gas and solid phases, respectively. The polarization energy $P$ contains electrostatic and electronic polarizations and molecular and lattice relaxations [6]. The magnitude of the polarization energy is in the range between 1 and 2 eV, [7] and the molecular and lattice relaxations contribute to its 5%–10% [8]. Although Eq. (1) still appears in the recent literature [6,9], it should be updated, taking recent advances into account as schematically shown in Fig. 1.

When Eq. (1) was established, it was assumed that the intermolecular interaction was so small that the bandwidth of organic solids was negligible [2] Since the 1990s, however, the intermolecular energy band dispersion was experimentally observed for some organic solids using energy-dependent and angle-resolved photoemission spectroscopy (PES) [10,11]. The bandwidth in pentacene, for example, is reported to be about 0.5 eV [12–18]. This means that $I_s$ and $A_s$ should include contributions $w_+$ and $w_-$ from the bandwidth of highest occupied molecular orbital (HOMO) and lowest unoccupied molecular orbital (LUMO)-derived bands, respectively.

In 2008, it was reported that the ionization energy $I_s$ in organic molecular films depends on the molecular orientation [19]. The difference of $I_s$ between the lying and standing orientations with respect to the substrate surface is on the order of 0.5 eV [19–23]. The origin of the orientation dependence is explained by the surface dipole $d$ formed by collective action of the anisotropic charge distribution in the molecule [22]. However, there is no experimental evidence for the existence of the surface dipole.

The above-mentioned "solid-state effects" have been discussed so far only for the occupied states (and $I_s$), based on experimental data obtained using PES, and not for the unoccupied states (and $A_s$) because of the lack of experimental techniques capable of measuring such small differences in the unoccupied states (and $A_s$). Recently, we have developed an experimental method called low-energy inverse photoemission spectroscopy (LEIPS) [24] which is an advanced version of the inverse photoemission spectroscopy (IPES). We have so far determined $A_s$ of several organic materials with a precision

*Corresponding author: hyoshida@chiba-u.jp; Present address: Graduate School of Advanced Integrated Science, Chiba University, 1-33 Yayoi-cho, Inage-ku, Chiba-shi 263-8522, Japan.

 

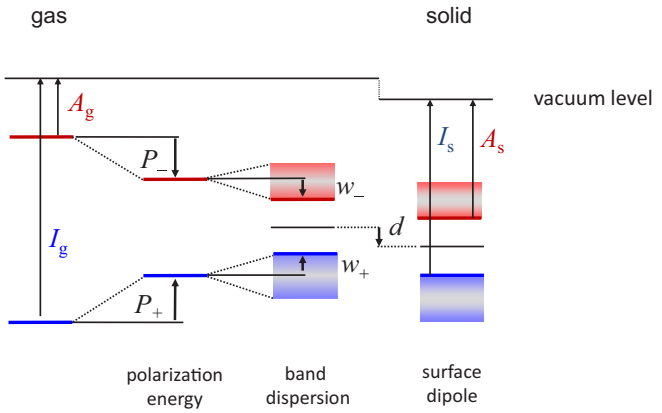


FIG. 1. (Color online) Schematic energy level diagram showing the ionization energy and electron affinity in the gas and solid phases.

of 0.1 eV [24–32]. Further, we have demonstrated that the precisely determined $A_s$ as well as $I_s$ allows us to distinguish the contribution of the polarization energy to the energy level change induced by the thermal crystallization of organic film of [6,6]-phenyl-$C_{61}$-butyric acid methyl ester (PCBM) [33]. By extending this idea, it should be possible to distinguish such effects as the polarization energy, band dispersion, and surface dipole; the electronic polarization energy and band dispersion primarily decrease $I_s$ and increase $A_s$, while the surface dipole causes a rigid shift of the energy levels, i.e., a systematic increase (or decrease) of both $I_s$ and $A_s$. Further discussion can be made with the aid of theoretical calculation of the polarization energies, $P_+$ and $P_-$ (these in a pair will be expressed as $P_\pm$ hereafter). Considering $I_s$ and $A_s$ in pairs will give more precise consideration than $I_s$ alone.

In this study, we show that electron affinities $A_s$ in organic molecular films depend on the molecular orientation using LEIPS. Combined with the other energy parameters evaluated according to the literature, we discuss the contribution of polarization energy, band dispersion, and molecular orientation to the energy levels in organic solids based on three models describing the gas-solid differences in the $I$ and $A$ values. We adopted pentacene (PEN) and perfluoropentacene (PFP) thin films because both show a large orientation dependence in $I_s$ [21] as well as the large band dispersion [12–18,35,36]. Their orientation dependence of $I_s$ is similar in magnitude but opposite in direction between PEN and PFP. Thus, comparison of the energy parameters between the gas and solid phases for PEN and PFP will provide us with a unique opportunity to discuss the solid-state effects, particularly, the band dispersion and the molecular orientation.

## II. EXPERIMENT

PEN (Aldrich) was purified with several cycles of vacuum sublimation. PFP (Kanto Denka Kogyo Co., LTD., sublimed in the factory) was used as received. Thin films of PEN and PFP were prepared with vacuum deposition on substrates kept at room temperature under the base pressure below $1 \times 10^{-6}$ Pa, while the molecular orientation was controlled by optimizing substrates and deposition rates. The materials were deposited on highly oriented pyrolytic graphite (HOPG) at a deposition rate of 1 nm $min^{-1}$ to obtain the lying orientation, and on naturally oxidized Si ($SiO_2$) surfaces at a deposition rate of $0.05 - 1$ nm $min^{-1}$ for the standing orientation. The substrates were heated at 400 °C beforehand for 16 h *in vacuo* to clean the surface. The molecular orientation was confirmed by observing the film morphology using atomic force microcopy [34,37–39] after the LEIPS measurements (see Supplemental Material [40]).

LEIPS measurements were carried out without exposing the samples to air. The experimental setup for LEIPS has been reported elsewhere [41]. To avoid sample damage, the kinetic energy of incident electrons was restricted to less than 5 eV. The electron current densities ranged between $2 \times 10^{-7}$ and $2 \times 10^{-5}$ A $cm^{-2}$. Under these experimental conditions, the same IPES profiles were obtained for repeated scans, confirming that sample damage was negligible. The emitted photons were focused on a photon detector consisting of an optical bandpass filter and a photomultiplier tube. The overall energy resolution was estimated to be 0.3 eV. The vacuum level of the sample was determined as the peak energy of the first derivative of the sample current. We confirmed that the LEIPS spectra depend on neither the thickness of the films nor the incident currents (see Figs. 9 and 10 in Appendix A).

## III. CALCULATION

The polarization energy was calculated based on the charge response kernel (CRK) model (see Supplemental Material [42], and also [43–45]) as the energy difference between a neutral lattice and a lattice with a molecular ion [6,46–48]. The electronic polarization effect was treated as the charge redistribution within each molecule following the CRK model. The calculation was made for a polarizable molecular cluster with its radius $R$ from the central molecular ion, surrounded by infinite nonpolarizable molecules (Fig. 2). A spherical cluster was employed for the calculation of polarization energies of bulk $P_\pm$, while a double-layer disk cluster was applied for film $P_\pm^{\mathrm{film}}$. The polarization energies were obtained by extrapolating $R$ to infinity. In the case of the film calculation, the substrate effect was included by placing image charges.

The energy band calculation of PFP was made for the crystal structures reported for the films on $SiO_2$ [34] and HOPG [36] using CASTEP code on the Material Studio program (Accelrys). The Perdew-Burke-Ernzerhof (PBE) functional version of the

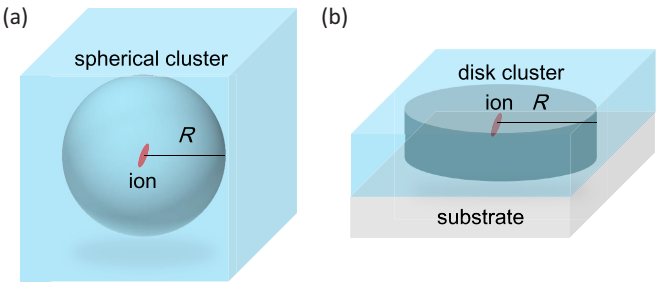


FIG. 2. (Color online) Schematics of the clusters used for the calculation of the polarization energies for (a) the bulk and (b) the thin film.

generalized gradient approximation (GGA) for the exchange-correlation energy was used. The plane-wave basis set with the cutoff energy of 370 eV was applied.

## IV. RESULTS AND DISCUSSION

### A. Ionization energies and electron affinities of PEN and PFP

Figure 3 shows LEIPS spectra of 10-nm-thick films of PEN and PFP measured at a photon energy of 4.38 eV (4.89 eV for the PFP in the standing orientation). The electron affinities were determined from the spectra taken at different photon energies in the range of 3.20–4.89 eV (shown in Figs. 11 and 12) to reduce the systematic error [24]. The results are shown in Fig. 3. The $A_s$ value of PEN determined previously, 2.7 eV [26], turned out to be an intermediate value between the standing and lying orientations. This is likely because the PEN film was formed on a rough ITO surface where the molecular orientation was not well defined.

When the molecular orientation changes from the standing to the lying orientation, the electron affinity $A_s$ increases by 0.79 eV for PEN and decreases by 0.54 eV for PFP, as in the case of the ionization energy $I_s$ [21]. Thus the band gap $E_g(= I_s - A_s)$, 2.3–2.6 eV for PEN and 2.4–2.5 eV for PFP, is nearly independent of the molecular orientation. Notably, the vacuum levels do not depend on the molecular orientation. We observed the variations of at most 0.15 eV from sample to sample which is substantially smaller than the orientation-dependent differences in $I_s$ and $A_s$.

The reported values of the ionization energy and electron affinity in the gas phase, $I_g$ and $A_g$, respectively, and $I_s$ for PEN and PFP are evaluated (Appendix B). $I_g$ for PEN and PFP determined by photoelectron spectroscopy are reported as 6.589 eV [49] and 7.50 eV [35], respectively. The $A_g$ value for PEN is reported to be 1.392 eV determined by ion-molecule reaction equilibrium [50,51]. As no experimental data are available for the electron affinity in the gas phase $A_g$ of PFP, we employ the calculated value of 2.66 eV [52] because the accuracy of the calculations for isolated molecules appeared to be sufficiently high, as judged from the calculated $A_g$ for PEN and $I_g$ for PEN and PFP which agree quantitatively with the corresponding experimental data (Table I). Further, the $A_g$ values for PFP calculated by different research groups are in close agreement. There are many reports on the ionization energy in the solid state $I_s$ of PEN and PFP as listed in Tables II and III, respectively. We selected the values for the sample film with well-defined orientation and the thickness exceeding 5 nm as discussed in Appendix A 1 (except for 3.6 nm for PFP with standing orientation). Finally, we evaluated $I_s$ as 4.90 eV [53–57] (standing) and 5.45 eV [58–60] (lying) for PEN, and $I_s$ = 6.65 eV [21,53] (standing) and 6.00 eV [36] (lying) for PFP.

### B. Polarization energies for the bulk material

We have calculated the polarization energies $P_+$ and $P_-$ for bulk materials using the CRK theory [43–45]. While PEN has several polymorphs [61] the calculated $(P_+ + P_-)$ for the different polymorphs vary less than 0.01 eV (see Supplemental Material [62]). Thus we made the calculation for the single-crystal phase. The calculated polarization energy for the cluster is plotted against the reciprocal of the cubic root of the cluster size $M$ in Fig. 4. While the unit cell of PEN contains the two crystallographically inequivalent molecules, the polarization energies for each site are the same within the accuracy of the present calculation. We obtained the polarization energies for the bulk material by extrapolating the radius of the cluster, which is proportional to $M^{-1/3}$, to infinity. The results are $P_+ = 0.46$ eV and $P_- = 1.35$ eV for PEN, and $P_+ = 1.53$ eV and $P_- = 0.09$ eV for PFP. Both $P_+$ and $P_-$ are largely different between PEN and PFP. This can be explained by the opposite direction of the static quadrupole moment between the PEN and PFP molecules [6,63,64]. Note that, when the nonpolarized molecules outside of the cluster are not included, the values are in excellent agreement with the recently reported values [9] suggesting that the accuracy of the calculated charge distribution using the CRK model is high and that the difference between the present and the previous values [9] depends on the structure of the cluster employed (see Supplemental Material [65]).

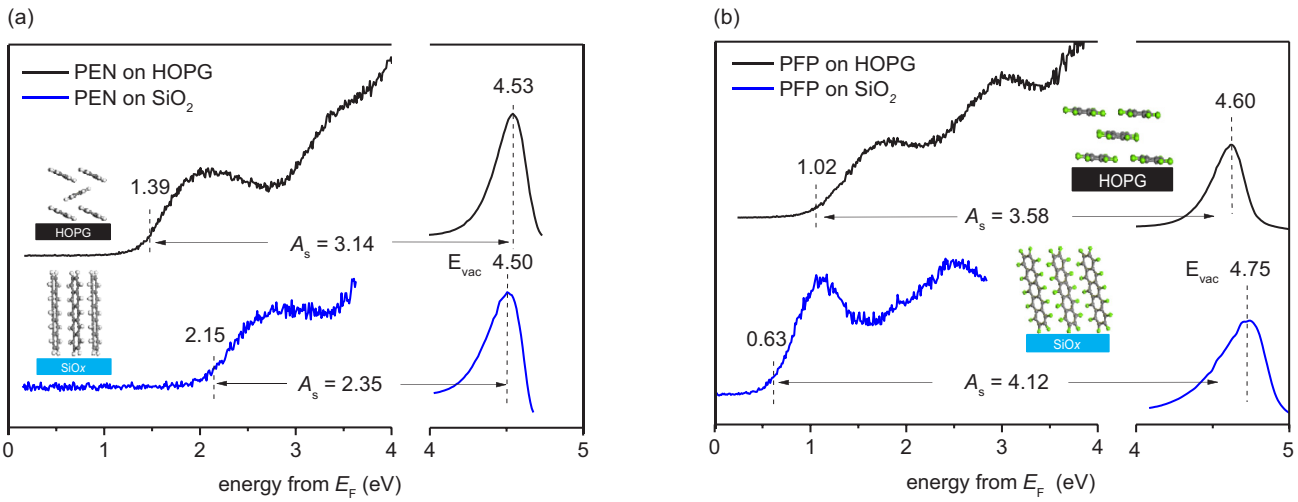


FIG. 3. (Color online) LEIPS spectra of (a) pentacene (PEN) and (b) perfluoropentacene (PFP) on HOPG and $SiO_2$ together with the first derivative of the sample current to determine the vacuum level $E_{vac}$.

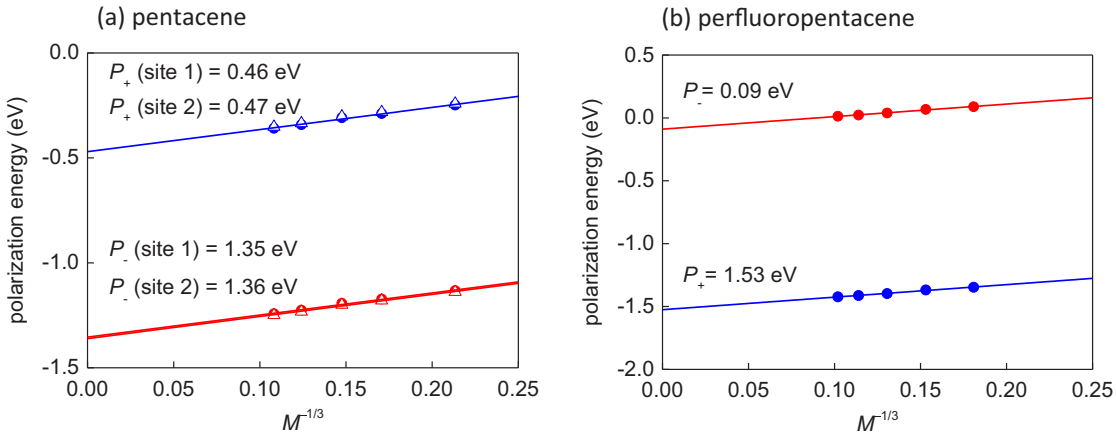


FIG. 4. (Color online) The polarization energies calculated for the spherical cluster, $P_+$ (blue circles and triangles) and $P_-$ (red circles and triangles), are plotted against the reciprocal of the cubic root of the cluster size, $M^{-1/3}$, for (a) pentacene (PEN) and (b) perfluoropentacene (PFP). We apply linear regression (solid line) on our data and $P$ for bulk materials are derived from the intercepts. There are two inequivalent molecules in a unit cell of the pentacene single crystal which are denoted as site 1 and 2.

Using the data of the energy levels and polarization energies presented above, we assess the validity of Eq. (1). Here we discuss the sum $(P_+ + P_-)$ instead of separate $P_+$ and $P_-$ values to avoid the effect of molecular orientations. The $(P_+ + P_-)$ value calculated using the CRK model is 1.81 eV for PEN and 1.62 eV for PFP, whereas the values estimated from Eq. (1) $(P_+ + P_- = I_g - A_g - I_s + A_s)$ are 2.6 − 2.9 eV for PEN and 2.4 eV for PFP. The CRK calculation gives the values about 1 eV smaller than the predicted values from Eq. (1). We anticipate that such differences can be explained by the energy levels broadened due to the band dispersion.

### C. Evaluation of the bandwidths

The energy band structure varies significantly for the polymorphs [66]. The crystallographic structures of the PEN films on $SiO_2$ [37] and graphene [67] are identified with the known structures of the thin film (interlayer distance $d_{001} = 1.54$ nm) [68] and single-crystal ($d_{001} = 1.41$ nm) [69–71] phases, respectively. The PFP film on $SiO_2$ [34,72] has a herringbone motif and identical structure to the single crystal [73] while that on graphene is characterized by $\pi$ stacking and is thought to be unique to the film [36]. Using x-ray diffraction, we confirmed that the structure of the PEN thin films on

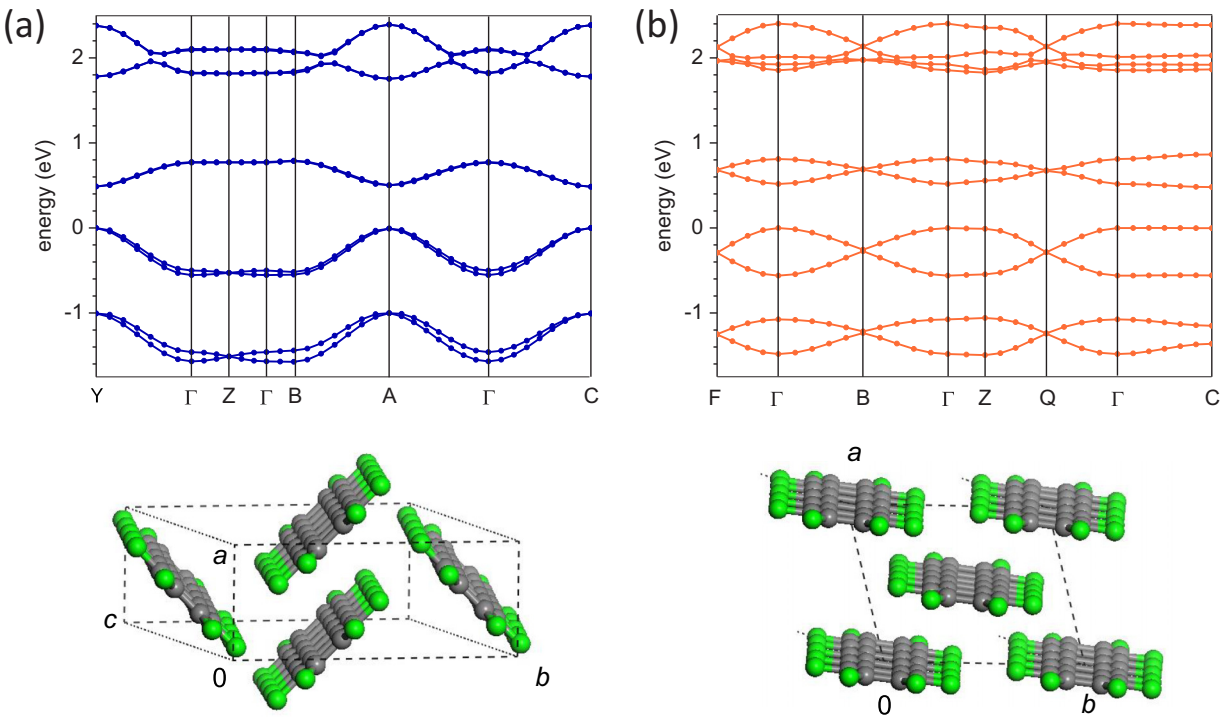


FIG. 5. (Color online) Calculated band structures of the PFP films on (a) $SiO_2$ and (b) HOPG for the HOMO-1, HOMO, LUMO, LUMO + 1, LUMO + 2 regions together with the crystallographic structures. Points of high symmetry in the first Brillouin zone are labeled: Γ (0,0,0), A (0.5,0.5,0), B (0.5,0,0), C (0,0.5,0.5), F (0,0.5,0), Y (0,0.5,0), and Z (0,0,0.5).

HOPG is the same as that on a graphene surface as shown in Fig. 13.

Band dispersion has been observed using angle-resolved PES only for the HOMO-derived level of PEN. The bandwidths for the identified polymorphs are 0.46 eV for the bulk phase [13] and 0.7 eV for the thin-film phase [17]. On the other hand, the calculated bandwidths of PEN in the bulk and thin-film phases are 0.37 and 0.60 eV [66], respectively, in good agreement with the experimental values. Further, the calculated band structures obtained using the different functional and basis sets agree quantitatively with each other [18,66,74–82]. We therefore use the calculated bandwidths for further discussions. The data from the literature [66] are used for PEN while the band structures of PFP were calculated in this study. From the calculated band structures shown in Fig. 5, the bandwidths are determined to be 0.554 eV (HOMO) and 0.308 eV (LUMO) for the films on $SiO_2$ (herringbone), and 0.561 eV (HOMO) and 0.385 eV (LUMO) for the film on HOPG ($\pi$ stacking).

### D. Interpretation of the ionization energy and electron affinity based on the bulk polarization energy and bandwidth

From the discussions above (also see Fig. 1), Eq. (1) is rewritten, taking into account the effects of band dispersion $w_+$ and $w_-$ for the HOMO and LUMO bands, respectively, and the surface dipole $d$,

$$\begin{aligned} I_s &= I_g - P_+ - w_+ + d, \\ A_s &= A_g + P_- + w_- - d. \end{aligned} \tag{2}$$

The contribution of band dispersion $w_+(w_-)$ is taken as the top (bottom) of the HOMO (LUMO) band with respect to the band center. In the case of PFP, the energy band structures are well approximated by the one-dimensional tight-binding model (cosine curve) [35,36]. Thus, $w_+$ and $w_-$ are half bandwidths of the HOMO and LUMO bands, respectively. The energy band structure of PEN is two dimensional and the middle of the band does not correspond to the band center [66]. In the context of this work, the center energy means that the energy level converges at the limit of zero intermolecular orbital interaction. The energy band of PEN calculated based on the density functional theory (DFT) is fitted to the tight-binding model and the transfer integrals are set to zero so that the difference between the converged value and the top (bottom) of the HOMO (LUMO) band gives $w_+(w_-)$. Using the calculated band data [66], we derived $w_+ = 0.22\,\text{eV}$ and $w_- = 0.22\,\text{eV}$ for the film on $SiO_2$ (the thin-film phase) and $w_+ = 0.19\,\text{eV}$ and $w = 0.26\,\text{eV}$ for the film on HOPG (the single-crystal phase).

The energy levels thus obtained are summarized in Fig. 6. Starting from $I_g$ and $A_g$ in the gas phase, we take account of the electronic polarizations in the bulk $P_\pm$ and the bandwidths $w_\pm$ resulting in the band gaps $E_g$ of 2.9 eV for PEN and 2.8 eV for PFP. The experimentally determined band gap $E_g$ is satisfactorily reproduced by including the bandwidth. The difference of about 0.3 eV (except for 0.6 eV for PEN on HOPG) can be understood by other effects neglected in Eq. (2), such as the molecular and lattice relaxation contribution [8] and the lifetime broadening [11]. It is notable to compare the results with those of $C_{60}$ where the bandwidth is small and no

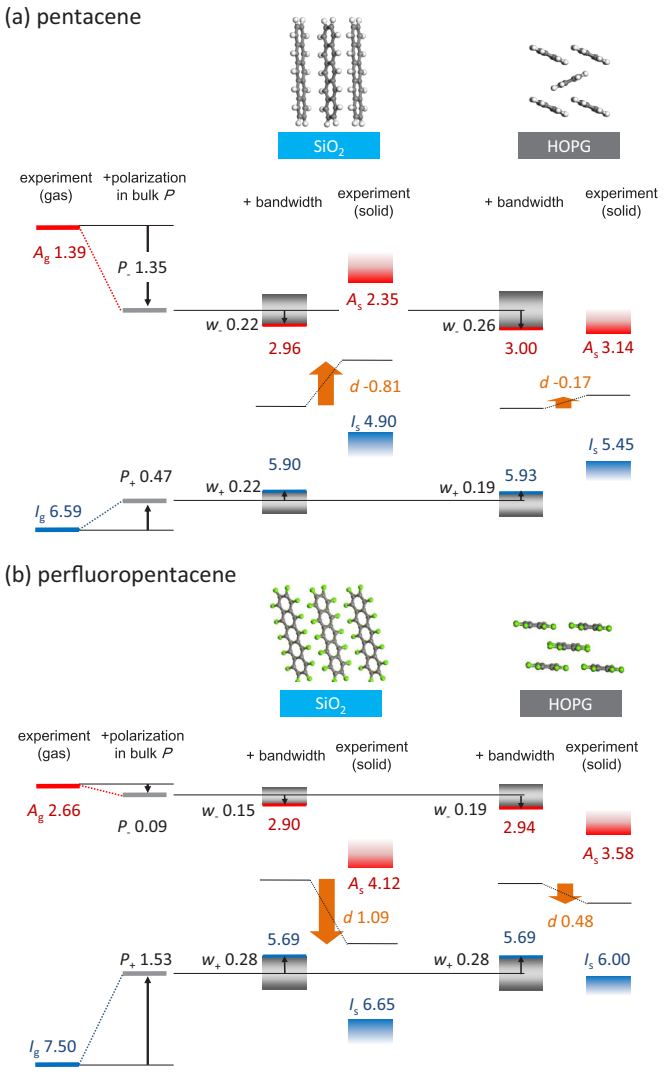


FIG. 6. (Color online) Energy level diagram of the ionization energy $I$ and electron affinity $A$ for the standing and lying molecular orientations of (a) pentacene (PEN) and (b) perfluoropentacene (PFP) films. The unit is eV. The $I_s$ and $A_s$ in the solid state are evaluated from those in the gas phase taking into account the polarization energy in the bulk $P_\pm$ and the contribution from the bandwidth $w_\pm$ according to Eq. (2). The horizontal bar in black indicates the mean value of the ionization energy and electron affinity. The difference in the mean value between evaluated and experiment is interpreted as the effect of surface dipole $d$.

orientation dependence is expected. The polarization energy determined as the energy level difference between the gas and solid phases [29,83], i.e., without including the bandwidth, is about 0.1−0.4 eV smaller than the calculated values [46]. The differences between the experimental and calculated values are comparable to the PEN and PFP case when the bandwidth is included.

As Fig. 6 shows, the ionization energy and electron affinity in the solid state predicted from the gas phase values, the polarization energy, and bandwidth are different from those obtained by PES and LEIPS measurements for the solid samples. We assumed the difference is due to the surface dipole $d$ and evaluated its magnitude as the difference in the mean

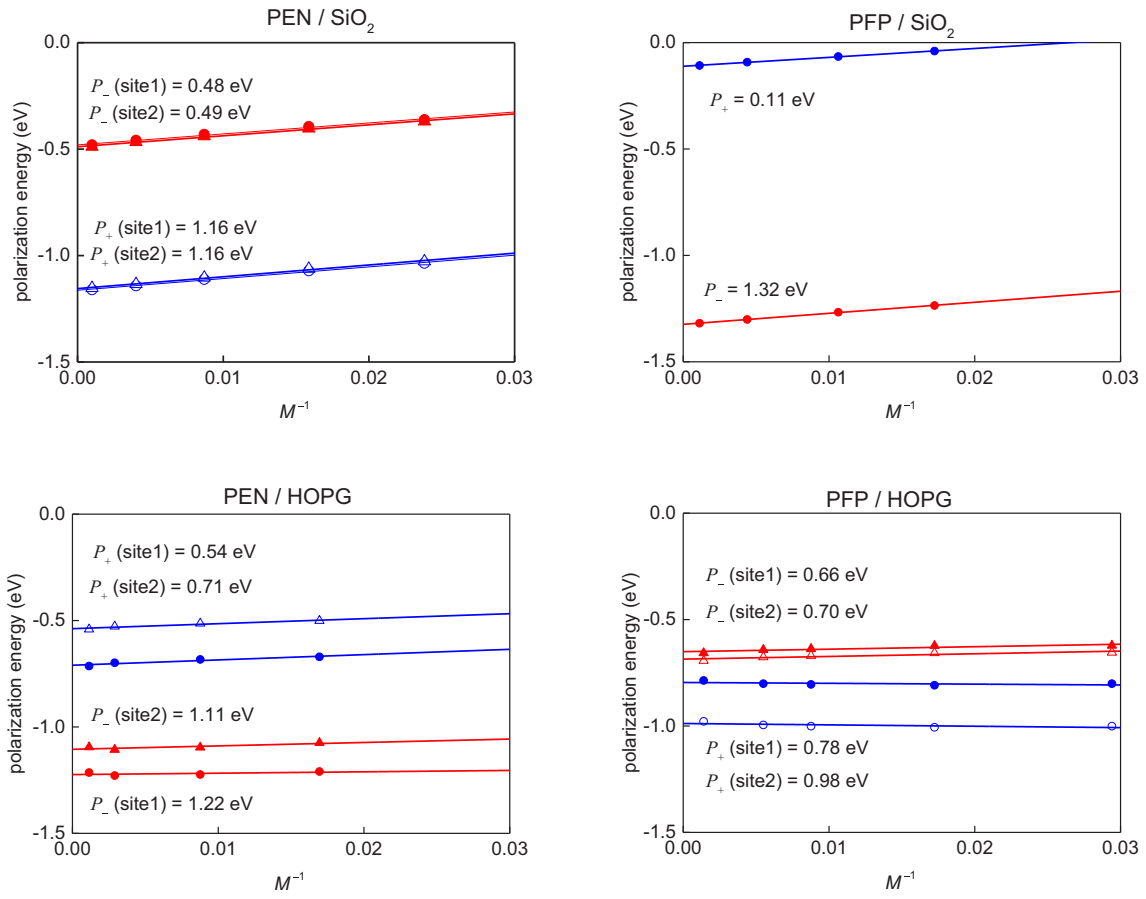


FIG. 7. (Color online) The polarization energies calculated for the disk clusters, $P_+$ (blue circles and triangles) and $P_-$ (red circles and triangles), are plotted against the reciprocal of the cluster size $M^{-1}$ for pentacene (PEN) and perfluoropentacene (PFP) with the standing ($SiO_2$) and lying (HOPG) orientations. We apply linear regression (solid line) on the data and $P$ for double-layer films are derived from the intercepts. There are two inequivalent molecules in a unit cell of the pentacene single crystal which are denoted as sites 1 and 2.

values of electron affinity and ionization energy. For PEN $d$ is $-0.8$ eV (standing) and $-0.2$ eV (lying), while for PFP 1.1 eV (standing) and 0.5 eV (lying). The trend appears to support the molecular electrostatics model proposed by Heimel *et al.* [22]. However, our observation of small difference in the vacuum level seems controversial; the vacuum level should change in association with the shift of ionization energy if the surface dipole $d$ depends on the molecular orientation. Actually, it is demonstrated that the surface dipole can be controlled by the surface segregation of a polar chain where the vacuum level varies associated with the change of the ionization energy [84,85].

### E. Polarization energy of the films

Recent theoretical studies predicted that the polarization energy $P$ depends on the "macroscopic shape" of the subject system [86] resulting in the orientation dependence of the ionization energy [6]. We therefore replace the polarization energy in the bulk $P_\pm$ in Eq. (2) with that in the film $P_\pm^{\rm film}$. Since only $P_+^{\rm film}$ has been calculated for PEN and PFP [6], we have calculated the polarization energies in the films with the different molecular orientations for both positive and negative charges, $P_+^{\rm film}$ and $P_-^{\rm film}$, respectively, as shown in Fig. 7. The $c^*$ (PEN) and $a^*$ (PFP) axes are normal to the surface of the $SiO_2$ substrate for the standing orientation, while the $b^*$ axes are normal to the HOPG surface for the lying orientation. For the lying orientation, the average values of site 1 and 2 are used. The calculated polarization energies $P_+$ for the positive ion film in Fig. 7 can be compared with the previously reported values [6]. Though the calculated values are in fairly good agreement, our values are always about 0.3 eV smaller, except for PEN with lying orientation, giving an estimate of the systematic error in the calculations. The band gaps are overestimated likely because the number of layer is limited and the substrate effect is not fully included in this calculation.

Based on the energy level evolution shown in Fig. 1, we derive the ionization energy and electron affinity for the thin films and compare them with the experimental values in Fig. 8. The model reproduces the experimental orientation-dependent differences remarkably with the disagreement as much as 0.1 eV; the observed orientation dependences of 0.65 eV for PEN and $-0.60$ for PFP, defined as average values of difference in the ionization energy and electron affinity, are in excellent agreement with the calculated values of 0.67 eV for PEN and $-0.69$ eV for PFP. The result clearly shows that the orientation dependence of $I_s$ and $A_s$ can be fully explained by the orientation-dependent polarization energy. The magnitude of the surface dipole $d$ may be a few tenths of eV but does not depend on the molecular orientation. The $I_s$ and $A_s$ are

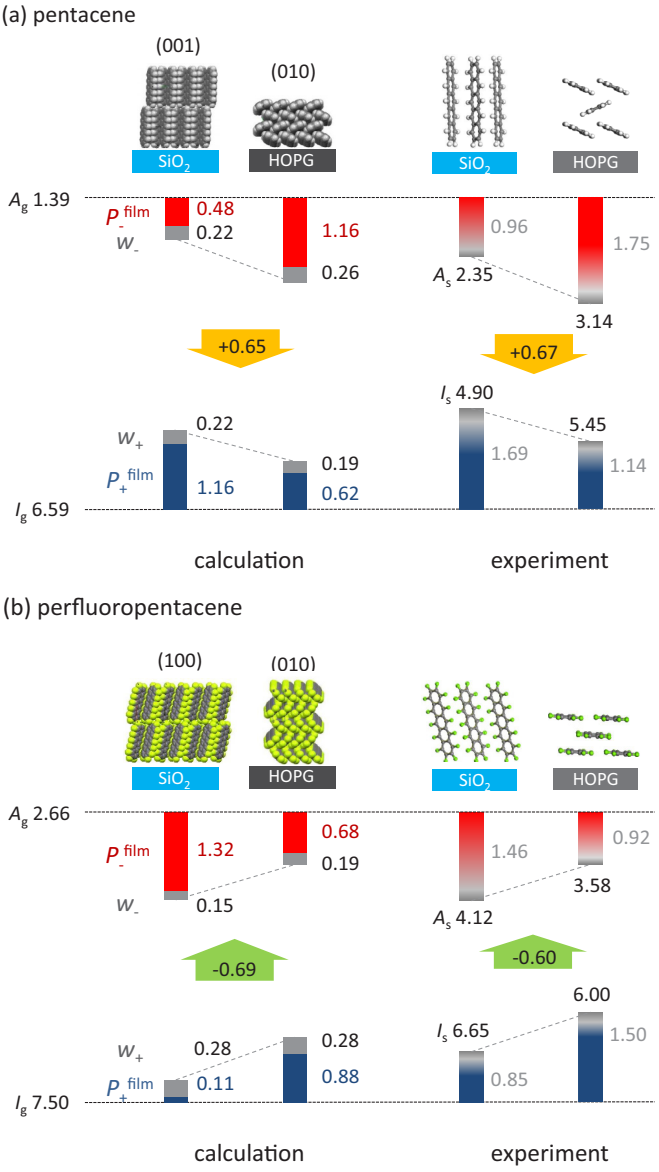


FIG. 8. (Color online) The molecular orientation dependence of ionization energy $I_s$ and electron affinity $A_s$ for (a) pentacene (PEN) and (b) perfluoropentacene (PFP) thin films are compared between the calculated and experimental values. The unit is eV. The calculations are based on the polarization energy in the film $P_{\pm}^{\rm film}$ with the contribution from the bandwidth $w_{\pm}$ according to Eq. (3). The diagrams are drawn with reference to the gas phase values.

therefore expressed as follows:

$$\begin{aligned} I_s &= I_g - P_+{}^{\rm film} - w_+, \\ A_s &= A_g + P_-{}^{\rm film} + w_-. \end{aligned} \tag{3}$$

The surface dipole discussed in Ref. [22] may account for the orientation dependence of $P$ in Eq. (2), i.e., the difference in the polarization energy between the bulk and thin film.

The experimental results show that the orientation dependence of ionization energy and electron affinity is quantitatively similar and in opposite direction between PEN and PFP. According to Ref. [6], the orientation dependence of the polarization energy originates from the electrostatic interaction, i.e., the charge-permanent quadrupole interaction in the nonpolar molecules. If this is the case, the direction of the orientation dependences is primarily determined by the molecular quadrupole, because the molecular and crystallographic structures are similar between PEN [68–71] and PFP [34]. The PEN and PFP have the permanent quadrupole tensors the components of which have similar absolute value but opposite sign; $Q_{xx} = 2.9$, $Q_{yy} = 2.8$, $Q_{zz} = -5.8 \times 10^{-39}$ C m$^2$ for PEN, $Q_{xx} = -3.8$, $Q_{yy} = -4.1$, $Q_{zz} = 7.9 \times 10^{-39}$ C m$^2$ for PFP, where $x$, $y$, and $z$ direct the molecular long axis, molecular short axis, and axis normal to the molecular plane, respectively [6]. The predicted orientation dependence between PEN and PFP based on the electrostatic interaction is consistent with the experimental observation, further supporting our conclusion.

### F. Localization of the charge carriers

Finally we will comment on the localization or delocalization of the charge carriers in the PEN solid. Regarding the behavior of charge carriers in organic semiconductors, the fundamental question remains open whether charges are localized on individual molecules or exhibit bandlike conduction [87,88]. As PEN shows a large bandwidth and high charge carrier mobility, the carrier transport in PEN is expected to be bandlike [89,90]. In the present study, on the other hand, the charge carrier is assumed to localize on a single molecule in the calculation of the polarization energy. When the charge carrier delocalizes, the polarization energy should decrease. This relation can be expressed by the Born equation, $P = (e^2/8\pi\varepsilon_0 r)(1 - 1/\varepsilon_r)$, where the elementary charge $e$ is confined in a sphere with the radius $r$ surrounded by a uniform dielectric medium with the relative permittivity $\varepsilon_r$; $\varepsilon_0$ refers to the permittivity of vacuum. The equation indicates that the polarization energy $P$ decreases linearly as a function of dimension $r$. The magnitude of $P$ may not be smaller than 0.5 eV, one half of the evaluated value in this work with the uncertainty considered. This fact suggests that the charge carriers in PEN and PFP are effectively localized on a single or at most a few molecules at room temperature. This picture is consistent with the conclusion of the previous experimental [91] and theoretical [92,93] studies.

## V. CONCLUSION

We have determined the molecular orientation-dependent values of $A_s$ for PEN and PFP thin films using low-energy inverse photoemission spectroscopy. The electronic state in an organic solid is considered as that of an isolated organic molecule perturbed by such solid-state effects as the polarization energy, bandwidth, and surface dipole. Combined with the other energy parameters evaluated using the literature data, we have determined the contribution of the solid-state effects based on three models represented by Eqs. (1)–(3). The first one [Eq. (1)] [1] only includes the polarization energy $P_{\pm}$ and underestimates the difference of the energy levels between the gas and solid phases. The second model [19,22] contains the polarization energy in the bulk $P_{\pm}$ and the effect of bandwidth $w_{\pm}$, and the dipole layer $d$ [Eq. (2)]. This model fails to explain the observed small vacuum level differences of at most 0.15 eV. In the third model [Eq. (3)], the polarization energy of the film $P_{\pm}^{\rm film}$ which depends on the molecular orientation and the bandwidth $w_{\pm}$ are considered. Only this model explains both the orientation-dependent energy levels ($I_s$ and $A_s$) and the small vacuum level shifts consistently.

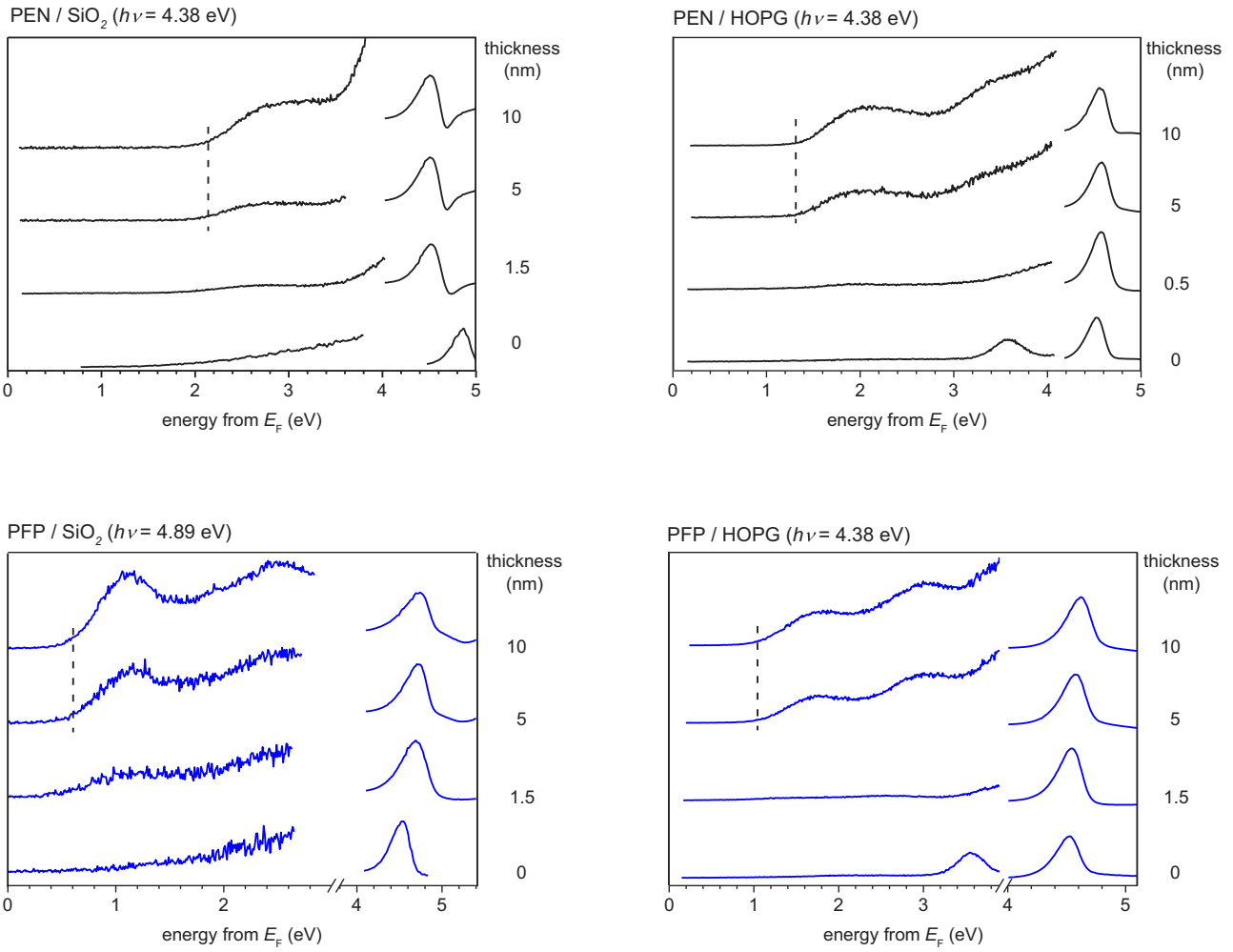


FIG. 9. (Color online) Thickness dependence of LEIPS spectra of PEN and PFP on $SiO_2$ and HOPG substrates. The spectra on the right in each panel are the first derivatives of sample currents, the peak of which give the vacuum levels.


## ACKNOWLEDGMENTS

The authors thank Dr. Koganezawa of Japan Synchrotron Radiation Research Institute for helping with the x-ray diffraction experiments. Computation time was provided by the SuperComputer System, Institute for Chemical Research, Kyoto University. This research was supported by Japan Science and Technology Agency (JST) PRESTO, and JSPS KAKENHI Grants No. 25410093 and No. 26288007 in parts.


## APPENDIX A: LOW-ENERGY INVERSE PHOTOEMISSION SPECTRA UNDER VARIOUS EXPERIMENTAL CONDITIONS

In order to determine the electron affinities of the sample materials precisely, we examined the dependence of the film thickness, incident electron current, and photon energy. Finally, the electron affinities are determined from the data taken for the 10-nm-thick films at the different photon energies.

### 1. Thickness dependence of LEIPS spectra of PEN and PFP

The LEIPS spectra were measured for the different thickness films at the photon energy 285 nm as shown in Fig. 9. We observed discernible effects from neither the substrate nor the sample charging in the range between 5 and 10 nm. When the PEN or PFP is deposited on $SiO_2$ substrate, vacuum level shifts by as much as 0.3 eV. On the HOPG substrate, the vacuum level shifts were below 0.05 eV.

### 2. Incident electron current dependence of LEIPS spectra of PEN and PFP

The LEIPS spectra were measured at the photon energy of 4.38 eV (4.89 eV only for PFP on $SiO_2$) with the incident electron current varied, ranging between 0.006 and 0.8 $\mu$A. As shown in Fig. 10, no discernible differences in the spectral line shape and the onset energy were observed, confirming the observed spectra are free from the sample charging.

### 3. Photon energy dependences of LEIPS spectra and determination of electron affinities

The LEIPS spectra were measured at different photon energies in the range between 3.20 and 4.89 eV as shown in Fig. 11. The similarity of the spectra shows that the spectra certainly reflect the density of unoccupied states and are free from the initial-state effects. The onset energies in the kinetic

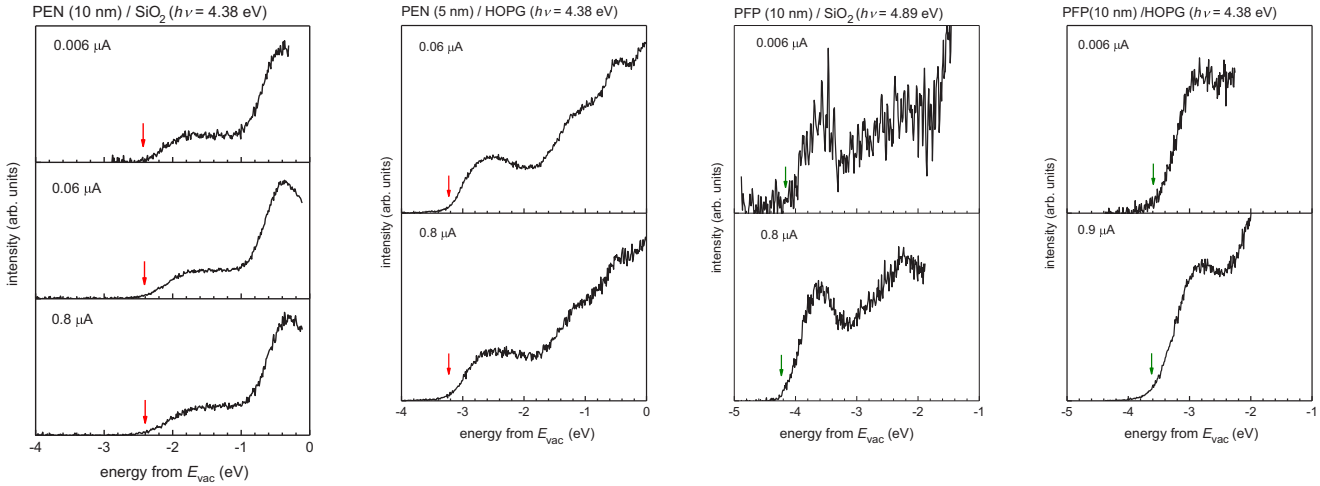


FIG. 10. (Color online) LEIPS spectra of PEN and PFP on the $SiO_2$ and HOPG substrates with the incident electron current varied by the second or third orders of magnitude. The sample current is indicated in each panel.

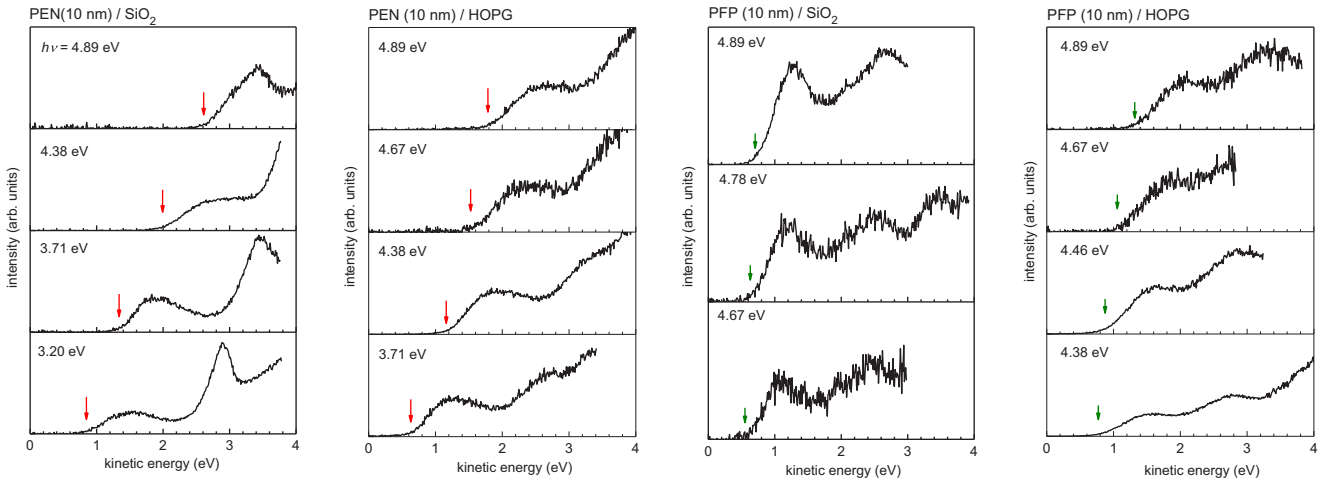


FIG. 11. (Color online) Photon energy dependences of LEIPS spectra of 10-nm-thick PEN and PFP films on the $SiO_2$ and HOPG substrates.

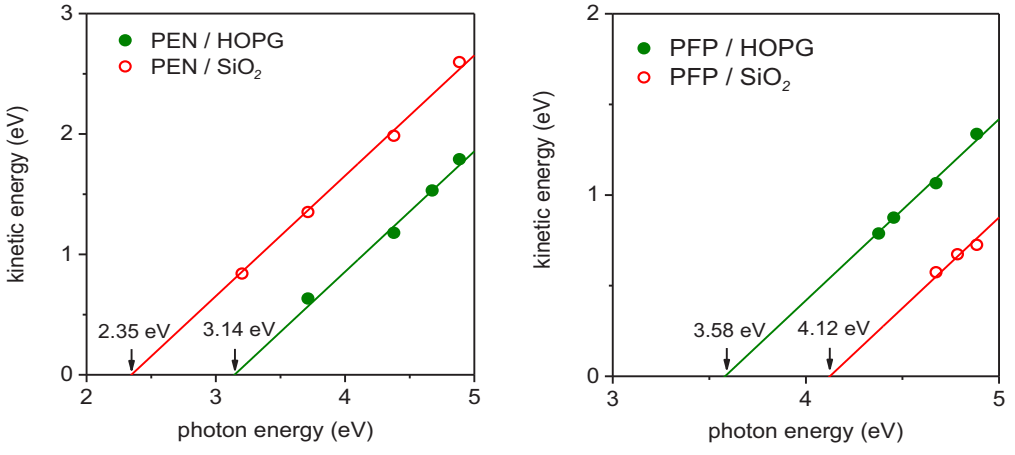


FIG. 12. (Color online) Onset energy vs photon energy of LEIPS spectra of 10-nm-thick PEN and PFP on $SiO_2$ and HOPG substrates.

TABLE I. The calculated adiabatic ionization energies and electron affinities for PEN and PFP taken from the literature.

| PEN | | PFP | | | |
|---|---|---|---|---|---|
| $A_g$ (eV) | $I_g$ (eV) | $A_g$ (eV) | $I_g$ (eV) | Method | Reference |
| 1.50 | 6.24 | 2.66 | 7.21 | HSE06/6-311++G** | [52] |
| 1.52 | 6.46 | 2.68 | 7.24 | B3LYP/6-311++G** | [6] |
| 1.491 | 6.126 | 2.779 | 7.122 | B3LYP/6-31++G**//6-31G** | [94] |
| 1.540 | | 2.854 | | B3LYP/ 6-311+G**//6-31G** | [95] |
| 1.592 | | 2.889 | | B3LYP/6-31+G*+ZPE | [95] |
| | | 2.790 | | B3LYP/DZP++ | [95] |
| 1.49 | 6.13 | 2.78 | 7.12 | B3LYP/6-31++G**//B3LYP/6-31G** | [35] |
| 1.479 | | | | B3LYP/6-31+G* | [96] |
| 1.35[a] | 6.59[b] | | 7.50[c] | Experiment | – |

[a]Reference [50].
[b]Reference [49].
[c]Reference [35].

TABLE II. The ionization energies of the pentacene (PEN) films taken from the literature.

| $I_s$ (eV) | Orientation[a] | Orientation analysis | Thickness (nm) | Substrate | Reference |
|---|---|---|---|---|---|
| $4.90 \pm 0.02$ | Standing | | 20 | ITO | [57] |
| $4.95 \pm 0.03$ | | | Single crystal | – | [57] |
| 4.9 | (Standing) | | 15 | $SiO_2$ | [97] |
| $4.88 \pm 0.05$ | (Standing) | | 1 | ITO | [26] |
| $4.90 \pm 0.05$ | (Standing) | | 10, 20 | ITO | [26] |
| $4.78 \pm 0.1$ | Standing | | 2.7 | Poly Au | [56] |
| $4.85 \pm 0.1$ | Standing | | 4.9 | Poly Au | [56] |
| $4.83 \pm 0.1$ | Standing | | 7.1 | Poly Au | [56] |
| 5.25 | Lying (tilted by 29°) | NEXAFS | 7 | Graphene/SiC | [98] |
| 4.9 | Standing | XRD, GIXRD | 20 | $SiO_2$ | [36] |
| 4.93 | Standing | | 10 | $SiO_2$ | [54] |
| 4.69 | Standing | | 10 | $OTS/SiO_2$ | [54] |
| 5.15 | Lying | NEXAFS | 10 | Graphene | [67] |
| 5.19 | Lying | | Monolayer | Au(111) | [59] |
| 5.45 | Lying | | Multilayer | Au(111) | [59] |
| $4.9 \pm 0.1$ | Standing | XRD | 3.2 | $SiO_2$ | [53] |
| 5.6 | Lying | | Monolayer | HOPG | [99] |
| 5.15 | Lying | UPS angle dependence | Monolayer | Au(111) | [58] |
| 5.45 | Lying | UPS angle dependence | Multilayer | Au(111) | [58] |
| $4.74 \pm 0.04$ | Standing | | 1−1.6 | ITO | [100] |
| $4.72 \pm 0.04$ | Standing | | 1–1.6 | $SiO_2$ | [100] |
| 5.45 | Lying | | −3 | HOPG | [60] |
| 5.15 | (Amorphous) | | −10 | HOPG | [60] |
| 4.77 | Standing | | 20 | $SiO_2$ | [60] |
| 5.1[b] | Standing | | 7.5 | Poly Au | [101] |
| 5.15[c] | Amorphous | XRD | 40–60 | Poly Au | [102] |
| 4.85[d] | Standing | XRD | 40–60 | Poly Au | [102] |

[a]The orientations indicated in parentheses are estimated by the present authors.
[b]The value is derived from the original figure in Ref. [101].
[c]The film was prepared at room temperature.
[d]The film was prepared on the substrate at the temperature of 80 °C.

TABLE III. The ionization energies of perfluoropentacene (PFP) in the solid phase taken from the literature.

| $I_s$ (eV) | Orientation | Orientation analysis | Thickness (nm) | Substrate | Reference |
|---|---|---|---|---|---|
| 6.18 | Lying | STM | Monolayer | HOPG (295 K) | [103] |
| 6.02 | Lying | STM | Monolayer | HOPG (53 K) | [103] |
| 6.0 | Lying | GIXRD, NEXAFS | 10 | HOPG | [36] |
| 5.60 | Lying | UPS angle dependence | 0.2 | Au(111) | [58] |
| 6.20 | Lying | UPS angle dependence | 1.5 | Au(111) | [58] |
| 6.20–6.40 | Lying | UPS angle dependence | 7 | Au(111) | [58] |
| 6.65 | Standing | XRD | 3.6 | $SiO_2$ | [53] |

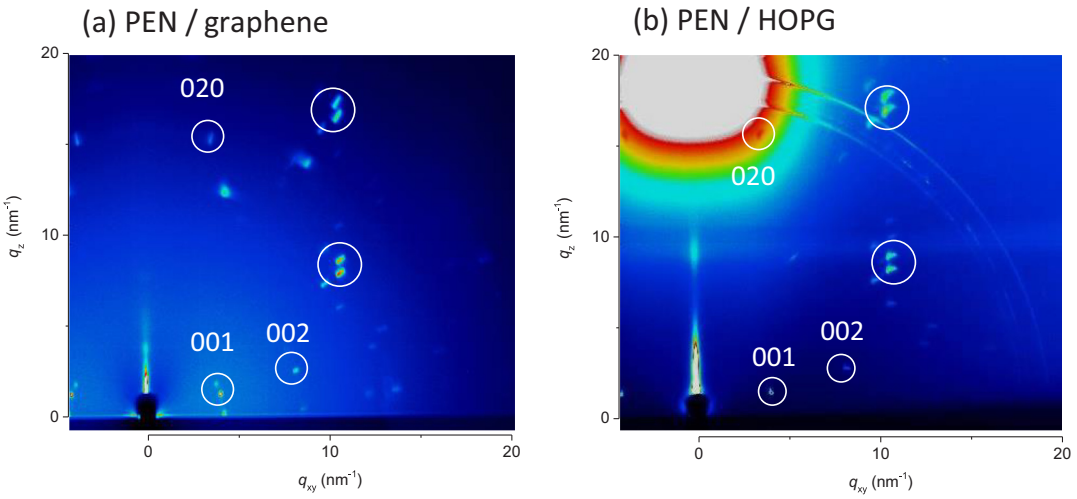


FIG. 13. (Color online) Grazing x-ray diffraction patterns of pentacene thin films on (a) graphene and (b) HOPG.

energy of the electron are plotted as a function of photon energy, and we apply linear regression with the slope of unity in Fig. 12. From the intercept, the electron affinities were determined. This procedure reduces the systematic error efficiently [24].

## APPENDIX B: COMPILED ENERGY PARAMETERS FOR PEN AND PFP

### 1. Compiled ionization energies and electron affinities for isolated PEN and PFP molecules

Since no experimental data are available, we use the calculated data on the electron affinity of PFP in the gas phase $A_g$. The calculated adiabatic ionization energies and electron affinities for PEN and PFP are listed in Table I. The evaluation of $I_g$ of PFP is described in the main text.

### 2. Compiled ionization energies of PEN and PFP in the solid phase determined using photoemission spectroscopy

There has been a large volume of data on the ionization energy of PEN and PFP using PES in the literature. The values as well as the molecular orientation, the method for analyzing the molecular orientation, and the thickness of the film and substrates for PEN and PFP are listed in Tables II and III, respectively.

## APPENDIX C: THE CRYSTALLOGRAPHIC STRUCTURE OF PEN ON HOPG AND GRAPHENE

The crystallographic structure of pentacene (PEN) on graphene is identified as the single-crystal phase (the interlayer space of $d_{001} = 1.41$ nm) [69–71] with the $b$ axis close to the normal to the substrate [67]. We examined the crystallographic structure and molecular orientation of PEN film on HOPG using the grazing incidence x-ray diffraction (GIXD). The GIXD measurement was carried out on the beam line BL19B2 at the SPring-8. A monochromatized x ray with the wavelength of 0.1 nm was incident to the sample surface with the angle of $0.07^\circ - 0.10^\circ$ and the diffraction was observed using a two-dimensional detector (PILATUS 300 K). Figure 13(a) shows the GIXD patterns of 10-nm-thick PEN on graphene which is similar to the previously reported result [67]. The 50-nm-thick PEN on HOPG in Fig. 13(b) shows at least seven distinct diffraction spots together with the intense diffraction from HOPG (0002). The diffraction patterns of the PEN on graphene and HOPG quantitatively agree with each other, showing that the PEN film on HOPG is of the single-crystal phase with the $b$ axis almost normal to the substrate.

[1] F. Gutmann and L. E. Lyons, in *Organic Semiconductors* (John Wiley and Sons, Inc., New York/Sydney, 1967).
[2] E. A. Silinsh, *Organic Molecular Crystals: Their Electronic States* (Springer, Berlin, Heidelberg, New York, 1980).
[3] K. Seki, H. Inokuchi, and Y. Harada, Chem. Phys. Lett. **20**, 197 (1973).
[4] K. Seki, Y. Harada, K. Ohno, and H. Inokuchi, Bull. Chem. Soc. Jpn. **47**, 1608 (1974).
[5] M. Pope and C. E. Swenberg, *Electronic Processes in Organic Crystals and Polymers* (Oxford University Press, New York, 1999).
[6] B. J. Topham and Z. G. Soos, Phys. Rev. B **84**, 165405 (2011).
[7] N. Sato, K. Seki, and H. Inokuchi, J. Chem. Soc., Faraday Trans. 2 **77**, 1621 (1981).
[8] E. Silinsh and V. Cápek, *Organic Molecular Crystals: Interaction, Localization, and Transport Phenomena* (American Institute of Physics, New York, 1994).
[9] S. M. Ryno, S. R. Lee, J. S. Sears, C. Risko, and J.-L. Bredas, J. Phys. Chem. C **117**, 13853 (2013).
[10] S. Hasegawa, T. Mori, K. Imaeda, S. Tanaka, Y. Yamashita, H. Inokuchi, H. Fujimoto, K. Seki, and N. Ueno, J. Chem. Phys. **100**, 6969 (1994).
[11] N. Ueno and S. Kera, Prog. Surf. Sci. **83**, 490 (2008).
[12] N. Koch, A. Vollmer, I. Salzmann, B. Nickel, H. Weiss, and J. P. Rabe, Phys. Rev. Lett. **96**, 156803 (2006).

[13] H. Kakuta, T. Hirahara, I. Matsuda, T. Nagao, S. Hasegawa, N. Ueno, and K. Sakamoto, Phys. Rev. Lett. **98**, 247601 (2007).

[14] S. Berkebile, P. Puschnig, G. Koller, M. Oehzelt, F. P. Netzer, C. Ambrosch-Draxl, and M. G. Ramsey, Phys. Rev. B **77**, 115312 (2008).

[15] H. Yamane, E. Kawabe, D. Yoshimura, R. Sumii, K. Kanai, Y. Ouchi, N. Ueno, and K. Seki, Phys. Status Solidi B **245**, 793 (2008).

[16] S. Berkebile, G. Koller, A. J. Fleming, P. Puschnig, C. Ambrosch-Draxl, K. Emtsev, T. Seyller, J. Riley, and M. G. Ramsey, J. Electron Spectrosc. Relat. Phenom. **174**, 22 (2009).

[17] M. Ohtomo, T. Suzuki, T. Shimada, and T. Hasegawa, Appl. Phys. Lett. **95**, 123308 (2009).

[18] S. Ciuchi, R. C. Hatch, H. Höchst, C. Faber, X. Blase, and S. Fratini, Phys. Rev. Lett. **108**, 256401 (2012).

[19] S. Duhm, G. Heimel, I. Salzmann, H. Glowatzki, R. L. Johnson, A. Vollmer, J. P. Rabe, and N. Koch, Nat. Mater. **7**, 326 (2008).

[20] W. Chen, H. Huang, S. Chen, Y. L. Huang, X. Y. Gao, and A. T. S. Wee, Chem. Mater. **20**, 7017 (2008).

[21] I. Salzmann, S. Duhm, G. Heimel, M. Oehzelt, R. Kniprath, R. L. Johnson, J. P. Rabe, and N. Koch, J. Am. Chem. Soc. **130**, 12870 (2008).

[22] G. Heimel, I. Salzmann, S. Duhm, and N. Koch, Chem. Mater. **23**, 359 (2011).

[23] C. G. Wang, A. J. Turinske, and Y. L. Gao, Appl. Phys. B: Lasers Opt. **113**, 361 (2013).

[24] H. Yoshida, Chem. Phys. Lett. **539-540**, 180 (2012).

[25] S. Fabiano, H. Yoshida, Z. Chen, A. Facchetti, and M. A. Loi, ACS Appl. Mater. Interfaces **5**, 4417 (2013).

[26] W. Han, H. Yoshida, N. Ueno, and S. Kera, Appl. Phys. Lett. **103**, 123303 (2013).

[27] Y. Ie, M. Karakawa, S. Jinnai, H. Yoshida, A. Saeki, S. Seki, S. Yamamoto, H. Ohkita, and Y. Aso, Chem. Commun. **50**, 4123 (2014).

[28] H. Yoshida, Anal. Bioanal. Chem. **406**, 2231 (2014).

[29] H. Yoshida, J. Phys. Chem. C **118**, 24377 (2014).

[30] H. Yoshida and K. Yoshizaki, Org. Electron. **20**, 24 (2015).

[31] N. Zhou, M.-G. Kim, S. Loser, J. Smith, H. Yoshida, X. Guo, C. Song, H. Jine, Z. Chen, S. M. Yoon, A. J. Freeman, R. P. H. Chang, A. Facchetti, and T. J. Marks, Proc. Natl. Acad. Sci. USA **112**, 7897 (2015).

[32] H. Yoshida, J. Electron Spectrosc. Relat. Phenom. (2015), doi:10.1016/j.elspec.2015.07.003.

[33] Y. Zhong, S. Izawa, K. Hashimoto, K. Tajima, T. Koganezawa, and H. Yoshida, J. Phys. Chem. C **119**, 23 (2015).

[34] I. Salzmann, S. Duhm, G. Heimel, J. P. Rabe, N. Koch, M. Oehzelt, Y. Sakamoto, and T. Suzuki, Langmuir **24**, 7294 (2008).

[35] M. C. R. Delgado, K. R. Pigg, D. Filho, N. E. Gruhn, Y. Sakamoto, T. Suzuki, R. M. Osuna, J. Casado, V. Hernandez, J. T. L. Navarrete, N. G. Martinelli, J. Cornil, R. S. Sanchez-Carrera, V. Coropceanu, and J. L. Bredas, J. Am. Chem. Soc. **131**, 1502 (2009).

[36] I. Salzmann, A. Moser, M. Oehzelt, T. Breuer, X. L. Feng, Z. Y. Juang, D. Nabok, R. G. Della Valle, S. Duhm, G. Heimel, A. Brillante, E. Venuti, I. Bilotti, C. Christodoulou, J. Frisch, P. Puschnig, C. Draxl, G. Witte, K. Mullen, and N. Koch, ACS Nano **6**, 10874 (2012).

[37] I. P. M. Bouchoms, W. A. Schoonveld, J. Vrijmoeth, and T. M. Klapwijk, Synth. Met. **104**, 175 (1999).

[38] J. Götzen, D. Käfer, C. Wöll, and G. Witte, Phys. Rev. B **81**, 085440 (2010).

[39] T. Breuer, I. Salzmann, J. Goetzen, M. Oehzelt, A. Morherr, N. Koch, and G. Witte, Cryst. Growth Des. **11**, 4996 (2011).

[40] See Supplemental Material at http://link.aps.org/supplemental/10.1103/PhysRevB.92.075145 for the AFM images of PEN and PFP films on HOPG and $SiO_2$.

[41] H. Yoshida, Rev. Sci. Instrum. **85**, 016101 (2014).

[42] See Supplemental Material at http://link.aps.org/supplemental/10.1103/PhysRevB.92.075145 for the details of the calculation method.

[43] A. Morita and S. Kato, J. Am. Chem. Soc. **119**, 4021 (1997).

[44] A. Morita and S. Kato, J. Chem. Phys. **108**, 6809 (1998).

[45] S. Iuchi, A. Morita, and S. Kato, J. Phys. Chem. B **106**, 3466 (2002).

[46] B. J. Topham, M. Kumar, and Z. G. Soos, Chem. Phys. Lett. **493**, 251 (2010).

[47] E. V. Tsiper, Z. G. Soos, W. Gao, and A. Kahn, Chem. Phys. Lett. **360**, 47 (2002).

[48] J. E. Norton and J. L. Bredas, J. Am. Chem. Soc. **130**, 12377 (2008).

[49] V. Coropceanu, M. Malagoli, D. A. da Silva Filho, N. E. Gruhn, T. G. Bill, and J. L. Brédas, Phys. Rev. Lett. **89**, 275503 (2002).

[50] L. Crocker, T. B. Wang, and P. Kebarle, J. Am. Chem. Soc. **115**, 7818 (1993).

[51] The ion-molecule reaction equilibrium gives the Gibbs free energy change. In order to determine the electron affinity (the enthalpy change), the entropy change is evaluated to be $-1.5$ e.u. See *NIST Chemistry WebBook*, available at http://webbook.nist.gov/chemistry/.

[52] G. Heimel, S. Duhm, I. Salzmann, A. Gerlach, A. Strozecka, J. Niederhausen, C. Burker, T. Hosokai, I. Fernandez-Torrente, G. Schulze, S. Winkler, A. Wilke, R. Schlesinger, J. Frisch, B. Broker, A. Vollmer, B. Detlefs, J. Pflaum, S. Kera, K. J. Franke *et al.*, Nat. Chem. **5**, 187 (2013).

[53] S. Duhm, I. Salzmann, G. Heimel, M. Oehzelt, A. Haase, R. L. Johnson, J. P. Rabe, and N. Koch, Appl. Phys. Lett. **94**, 033304 (2009).

[54] Y. M. Lee, J. W. Kim, H. Min, T. G. Lee, and Y. Park, Curr. Appl. Phys. **11**, 1168 (2011).

[55] I. Salzmann, G. Heimel, S. Duhm, M. Oehzelt, P. Pingel, B. M. George, A. Schnegg, K. Lips, R.-P. Blum, A. Vollmer, and N. Koch, Phys. Rev. Lett. **108**, 035502 (2012).

[56] P. Sehati, S. Braun, and M. Fahlman, Chem. Phys. Lett. **583**, 38 (2013).

[57] Y. Nakayama, Y. Uragami, M. Yamamoto, S. Machida, H. Kinjo, K. Mase, K. R. Koswattage, and H. Ishii, Jpn. J. Appl. Phys. **53**, 01AD03 (2014).

[58] N. Koch, A. Vollmer, S. Duhm, Y. Sakamoto, and T. Suzuki, Adv. Mater. **19**, 112 (2007).

[59] H. Yamane, K. Kanai, Y. Ouchi, N. Ueno, and K. Seki, J. Electron Spectrosc. Relat. Phenom. **174**, 28 (2009).

[60] H. Fukagawa, H. Yamane, T. Kataoka, S. Kera, M. Nakamura, K. Kudo, and N. Ueno, Phys. Rev. B **73**, 245310 (2006).

[61] C. C. Mattheus, A. B. Dros, J. Baas, G. T. Oostergetel, A. Meetsma, J. L. de Boer, and T. T. M. Palstra, Synth. Met. **138**, 475 (2003).

[62] See Supplemental Material at http://link.aps.org/supplemental/10.1103/PhysRevB.92.075145 for the comparison of the

($P_+ + P_-$) values between the thin-film and bulk phases of PEN.
[63] P. J. Bounds and R. W. Munn, Chem. Phys. **59**, 41 (1981).
[64] N. Sato, H. Inokuchi, and E. A. Silinsh, Chem. Phys. **115**, 269 (1987).
[65] See Supplemental Material at http://link.aps.org/supplemental/10.1103/PhysRevB.92.075145 for the caluculation without the nonpolarized molecule outside of the spherical cluster (Fig. S3) and a list of the calculated polarization energies for the bulk PEN and PFP (Table SI).
[66] H. Yoshida and N. Sato, Phys. Rev. B **77**, 235205 (2008).
[67] W. H. Lee, J. Park, S. H. Sim, S. Lim, K. S. Kim, B. H. Hong, and K. Cho, J. Am. Chem. Soc. **133**, 4447 (2011).
[68] H. Yoshida, K. Inaba, and N. Sato, Appl. Phys. Lett. **90**, 181930 (2007).
[69] D. Holmes, S. Kumaraswamy, A. J. Matzger, and K. P. C. Vollhardt, Chem. Eur. J. **5**, 3399 (1999).
[70] C. C. Mattheus, A. B. Dros, J. Baas, A. Meetsma, J. L. de Boer, and T. T. M. Palstra, Acta Crystallogr., Sect. C **57**, 939 (2001).
[71] T. Siegrist, C. Kloc, J. H. Schon, B. Batlogg, R. C. Haddon, S. Berg, and G. A. Thomas, Angew. Chem., Int. Ed. **40**, 1732 (2001).
[72] S. Kowarik, A. Gerlach, A. Hinderhofer, S. Milita, F. Borgatti, F. Zontone, T. Suzuki, F. Biscarini, and F. Schreiber, Phys. Status Solidi RRL **2**, 120 (2008).
[73] Y. Sakamoto, T. Suzuki, M. Kobayashi, Y. Gao, Y. Fukai, Y. Inoue, F. Sato, and S. Tokito, J. Am. Chem. Soc. **126**, 8138 (2004).
[74] R. C. Haddon, X. Chi, M. E. Itkis, J. E. Anthony, D. L. Eaton, T. Siegrist, C. C. Mattheus, and T. T. M. Palstra, J. Phys. Chem. B **106**, 8288 (2002).
[75] Y. C. Cheng, R. J. Silbey, D. A. da Silva, J. P. Calbert, J. Cornil, and J. L. Bredas, J. Chem. Phys. **118**, 3764 (2003).
[76] G. A. de Wijs, C. C. Mattheus, R. A. de Groot, and T. T. M. Palstra, Synth. Met. **139**, 109 (2003).
[77] M. L. Tiago, J. E. Northrup, and S. G. Louie, Phys. Rev. B **67**, 115212 (2003).
[78] R. G. Endres, C. Y. Fong, L. H. Yang, G. Witte, and C. Woll, Comput. Mater. Sci. **29**, 362 (2004).
[79] K. Doi, K. Yoshida, H. Nakano, A. Tachibana, T. Tanabe, Y. Kojima, and K. Okazaki, J. Appl. Phys. **98**, 113709 (2005).
[80] K. Hummer and C. Ambrosch-Draxl, Phys. Rev. B **72**, 205205 (2005).
[81] A. Troisi and G. Orlandi, J. Phys. Chem. B **109**, 1849 (2005).
[82] D. Nabok, P. Puschnig, C. Ambrosch-Draxl, O. Werzer, R. Resel, and D.-M. Smilgies, Phys. Rev. B **76**, 235322 (2007).
[83] K. Akaike, K. Kanai, H. Yoshida, J. Tsutsumi, T. Nishi, N. Sato, Y. Ouchi, and K. Seki, J. Appl. Phys. **104**, 023710 (2008).
[84] Q. Wei, K. Tajima, Y. Tong, S. Ye, and K. Hashimoto, J. Am. Chem. Soc. **131**, 17597 (2009).
[85] Y. Geng, Q. Wei, K. Hashimoto, and K. Tajima, Chem. Mater. **23**, 4257 (2011).
[86] E. V. Tsiper and Z. G. Soos, Phys. Rev. B **64**, 195124 (2001).
[87] N. Karl, Synth. Met. **133-134**, 649 (2003).
[88] A. Troisi, Chem. Soc. Rev. **40**, 2347 (2011).
[89] O. Ostroverkhova, D. G. Cooke, F. A. Hegmann, J. E. Anthony, V. Podzorov, M. E. Gershenson, O. D. Jurchescu, and T. T. M. Palstra, Appl. Phys. Lett. **88**, 162101 (2006).
[90] J. Takeya, J. Kato, K. Hara, M. Yamagishi, R. Hirahara, K. Yamada, Y. Nakazawa, S. Ikehata, K. Tsukagoshi, Y. Aoyagi, T. Takenobu, and Y. Iwasa, Phys. Rev. Lett. **98**, 196804 (2007).
[91] K. Marumoto, S.-I. Kuroda, T. Takenobu, and Y. Iwasa, Phys. Rev. Lett. **97**, 256603 (2006).
[92] A. Troisi and G. Orlandi, Phys. Rev. Lett. **96**, 086601 (2006).
[93] S. Fratini and S. Ciuchi, Phys. Rev. Lett. **103**, 266601 (2009).
[94] S. Chai, S. H. Wen, J. D. Huang, and K. L. Han, J. Comput. Chem. **32**, 3218 (2011).
[95] Y.-C. Chang, M.-Y. Kuo, C.-P. Chen, H.-F. Lu, and I. Chao, J. Phys. Chem. C **114**, 11595 (2010).
[96] A. Modelli, L. Mussoni, and D. Fabbri, J. Phys. Chem. A **110**, 6482 (2006).
[97] F. Bussolotti, S. Kera, K. Kudo, A. Kahn, and N. Ueno, Phys. Rev. Lett. **110**, 267602 (2013).
[98] X. Liu, A. Grueneis, D. Haberer, A. V. Fedorov, O. Vilkov, W. Strupinski, and T. Pichler, J. Phys. Chem. C **117**, 3969 (2013).
[99] M. Shionoiri, M. Kozasa, S. Kera, K. K. Okudaira, and N. Ueno, Jpn. J. Appl. Phys., Part 1 **46**, 1625 (2007).
[100] H. Fukagawa, S. Kera, T. Kataoka, S. Hosoumi, Y. Watanabe, K. Kudo, and N. Ueno, Adv. Mater. **19**, 665 (2007).
[101] F. Amy, C. Chan, and A. Kahn, Org. Electron. **6**, 85 (2005).
[102] N. Sato, K. Seki, H. Inokuchi, and Y. Harada, Chem. Phys. **109**, 157 (1986).
[103] S. Kera, S. Hosoumi, K. Sato, H. Fukagawa, S. Nagamatsu, Y. Sakamoto, T. Suzuki, H. Huang, W. Chen, A. T. S. Wee, V. Coropceanu, and N. Ueno, J. Phys. Chem. C **117**, 22428 (2013).